Hindawi
International Journal of Antennas and Propagation
Volume 2019, Article ID 4283010, 12 pages
https://doi.org/10.1155/2019/4283010

Research Article

High Isolation Millimeter-Wave Wideband MIMO Antenna for 5G Communication

Fei Wang, Zhaoyun Duan, Xin Wang, Qing Zhou, and Yubin Gong

School of Electronic Science and Engineering, University of Electronic Science and Technology of China, 610054 Chengdu, China

Correspondence should be addressed to Fei Wang; wfken231@163.com and Zhaoyun Duan; zhyduan@uestc.edu.cn

Received 26 October 2018; Revised 4 February 2019; Accepted 4 March 2019; Published 2 May 2019

Academic Editor: Shah Nawaz Burokur

A millimeter-wave wideband antenna is presented for the 5th generation applications. The operation band ranges from 24 GHz to 39 GHz which covers most of the Ka band. Furthermore, a 9×9 multiple-input-multiple-output (MIMO) antenna is developed. The high isolation is achieved without introducing external decoupling structures. The transmission coefficient is under −20 dB within only 0.4 mm space between antenna elements. The radiation pattern also shows the stability within the wide operation band. Both simulated and measured results show that this proposed MIMO antenna is suitable for the future wireless communications.

1. Introduction

With the rapid development of the wireless communication technology and increasing demand of the flexible applications, the next generation (5G) communication has become one of the hottest topics of the antenna industry [1–3]. Due to the limitation of the spectrum resources, current researches about 5G communication are mainly focusing on the millimeter-wave range. The frequency band around 28 GHz has attracted worldwide attention due to the resourceful continuous spectrum [4].

As one of the most important technologies of 5G communication, multiple-input-multiple-output (MIMO) technology is widely applied due to the high transmission rate and stable communication quality. It uses multiple antennas for transmitting and receiving signal in the wireless communications; thus, it can improve the capacity of the communication system and the utilization ratio of spectrum without increasing the transmitting power. As the miniaturization of the electronic equipment has become the major trend with the technology evolution, it requires the antenna with multiple elements to be placed in a limited area. At the same time, the MIMO system requires high isolation between different antennas, which in turn, needs more space between antennas [5, 6]. The big challenge for the researchers is to find the best balance between miniaturization and high isolation.

In current wireless communications, the 2×2 or 4×4 MIMO antennas are widely adapted. However, the 5G communication brings much higher requirement that an 8×8 or even a massive MIMO antenna is needed in 5G equipment. The increased amount of the MIMO antenna brings large challenge to all the researchers in the antenna industry. As one important factor in MIMO technology, the mutual coupling between antenna elements has been deeply studied. Generally, the decoupling structures such as parasitic elements [7], electronic band gap (EBG) [8], artificial metamaterials [9, 10], and filters are introduced to enhance the isolation. However, these decoupling structures will influence the antenna performance. Besides, other method such as orthogonal diversity [11] is also used to enhance the isolation. These methods still face problems when applying into the large-scale MIMO antenna and the uniform of the radiation patterns cannot be guaranteed.

In this paper, we present a novel wideband antenna for the 5G communications. The operation band of the proposed antenna ranges from 24 GHz to 39 GHz. Using symmetrical structure, the proposed antenna realizes stable radiation pattern in such a wide band. Based on it, the MIMO antennas are proposed and studied. Due to its unique structure, the

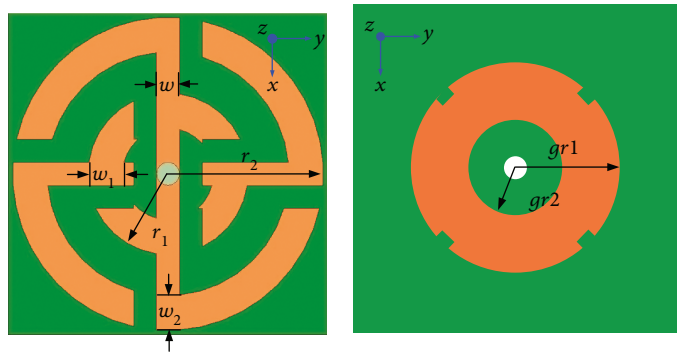

(a) (b)

Figure 1: Top (a) and bottom (b) of the proposed antenna.

Table 1: Dimensions (mm) of the proposed antenna.

w	w_1	w_2	r_1	r_2	gr_1	gr_2
1	1.5	1.5	3.5	6.8	4.5	2

high isolation between antenna elements is maintained when applying to large scale array.

2. Materials and Methods

2.1. Wideband Antenna Design. The proposed antenna is printed on a Rogers 4003C substrate with a relative permittivity of 3.4. The overall dimension of the proposed antenna is 14 mm × 14 mm × 0.8 mm. The top view and bottom view of the antenna are illustrated in Figures 1(a) and 1(b), respectively. The detailed dimensions of the proposed antenna are presented in Table 1.

The proposed antenna is developed from the normal monopole antenna. The radius of the outer circle is set as 6.8 mm. Therefore, the length of the longest branch is 11.1 mm which is close to the wavelength in free space at 26 GHz. The bended structure is used for minimizing the overall size of the antenna. The inner arc with a radius of 3.5 mm is added on the longest branch; therefore, the length of the inner arc is 8.9 mm which is close to the wavelength in free space at 32.5 GHz. The directions of the inner and outer arcs are opposite which can weaken the affection between two arcs. Furthermore, another same structure is added because the symmetrical structure can benefit the radiation performance such as radiation pattern and peak gain. To enhance the resonant at higher frequencies, the slots with the width of 0.2 mm are added on the inner circle branches. As shown in Figure 2(a), it can be seen that two main resonant frequencies appear at around 26 GHz and 32.5 GHz which agrees with our predicts.

Since the S_{11} is unsatisfactory at higher frequencies, two interleaved branches are added as parasitic elements on the both sides of the antenna for introducing the resonances at higher frequencies. The distance between the parasitic elements and the main structure is set as 1 mm to make sure that the parasitic branches can couple energy from the port. The length of the longest branch of the parasitic elements is 9.1 mm which is close to the wavelength in free space at 33 GHz.

The ground plane of the proposed antenna is designed as a ring. This is because the structures on the top side are mostly circular; other geometries will introduce unnecessary capacitances and inductances which lead to a deterioration of bandwidth. In the center of the substrate, a via hole is added for feeding. Considering the dimensions of the 2.92 mm K connector which can operate at up to 40 GHz, the radius of the via hole is set as 0.5 mm and the inner radius of the ground plane is set as 2 mm. Furthermore, the slots are etched on the ground plane for improving the impedance matching. After the parametric study shown in Figure 2(b), the width and length of the slots are 0.4 mm and 0.7 mm, respectively.

Using HFSS, the return loss of the proposed antenna with and without branches are presented in Figure 2. From Figure 2, it can be found that the interleaved branches can extend the operation bandwidth and decrease the return loss. It also can be found that two strong resonances appear at around 27 GHz and 34 GHz which show in good agreement with our predicts. The operation band ranges from 23.5 GHz to 36 GHz which covers most of the potential band of the 5G communication in the millimeter range.

The simulated radiation patterns are given in Figure 3. The radiation patterns show that the proposed UWB MIMO antenna has an approximate omnidirectional radiation. Besides, the change of the radiation patterns is slight within such a wide operation frequency band. Besides, the simulated gain of the proposed antenna is presented in Figure 3(c). It can be found that the maximum gain of the proposed antenna can reach 5 dBi at multiple frequencies.

2.2. MIMO Antenna Design. To investigate the potential in applying into various cases, the MIMO antennas with different distribution are studied. The geometry and simulated active S-parameters are presented in Figures 4(a) and 4(b), respectively. It can be clearly found that the active S-parameters of the proposed antenna show a stable performance which indicates that the mutual coupling maintains under a pretty low level while changing antenna element position. This fact implies that the geometry of the proposed MIMO antenna can be freely adjusted as required.

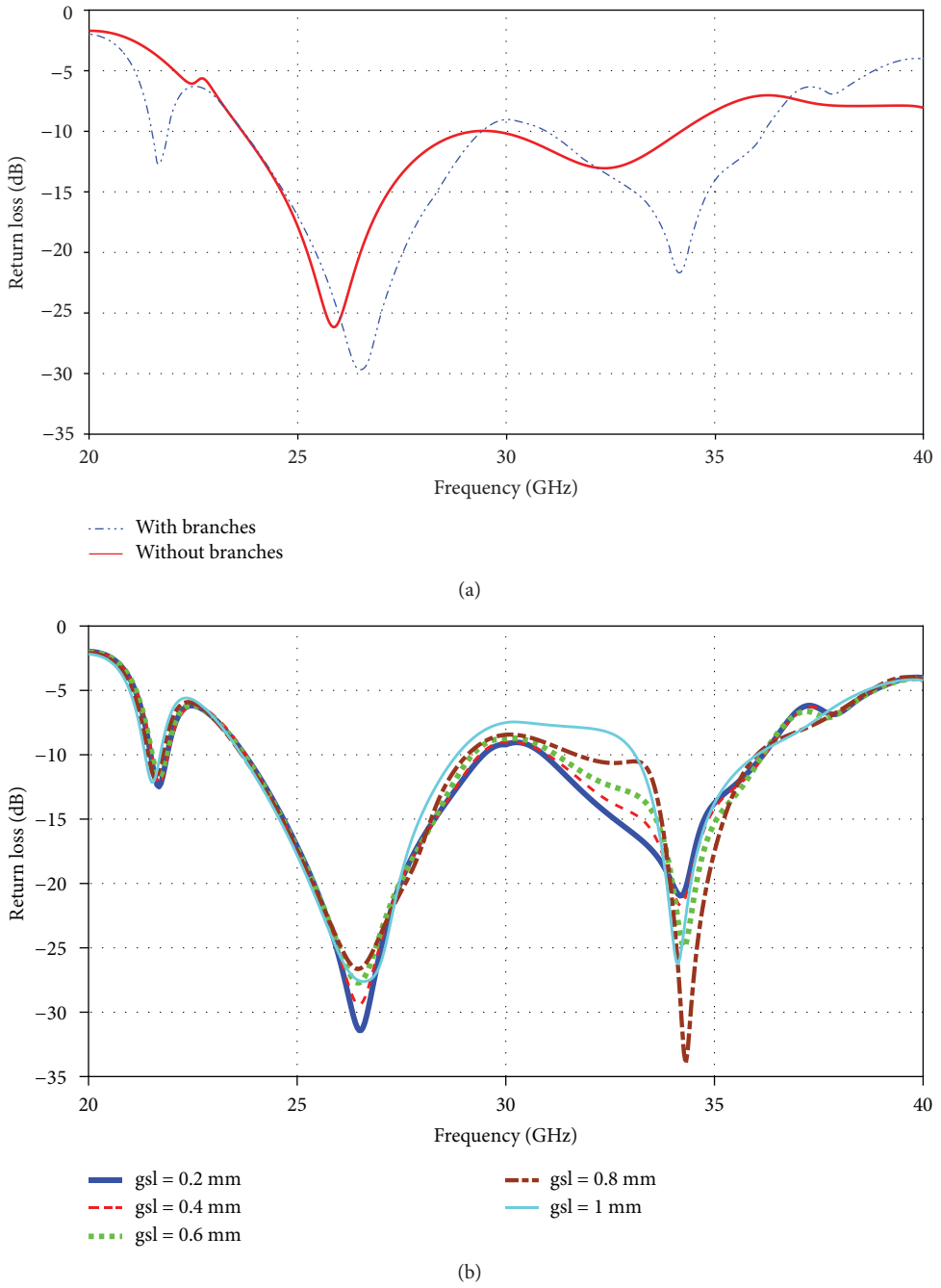

Figure 2: (a) Return loss of the proposed wideband antenna with and without branches, (b) parametric study of the small cuts on the ground plane.

To further investigate the mutual coupling between antenna elements, the current distribution on the MIMO antenna has been simulated and presented in Figure 5. Benefits from the cross structure of the proposed antenna, the directions of the coupling current on the nearby branches are different. Hence, the forward and reversed coupling currents can affect each other, and the power transmitted to the port is largely eliminated. Thus, it leads to a low mutual coupling, and the energy coupled to other elements is largely reduced.

Besides, due to the symmetry of the proposed antenna, the maximum value of the radiation pattern is on the plane which is perpendicular to the antenna. Hence, at 26 GHz, the radiation is mainly provided by the long branches on the y-direction as shown in Figure 5(a). Therefore, the radiation power reaches its peak on the yz plane which means the power coupled to the antenna elements 2 and 8 is under a pretty low level. However, for antenna elements 4 and 6, the distance between long branches is longer and the parasitic branches play a role of decoupling structure. The

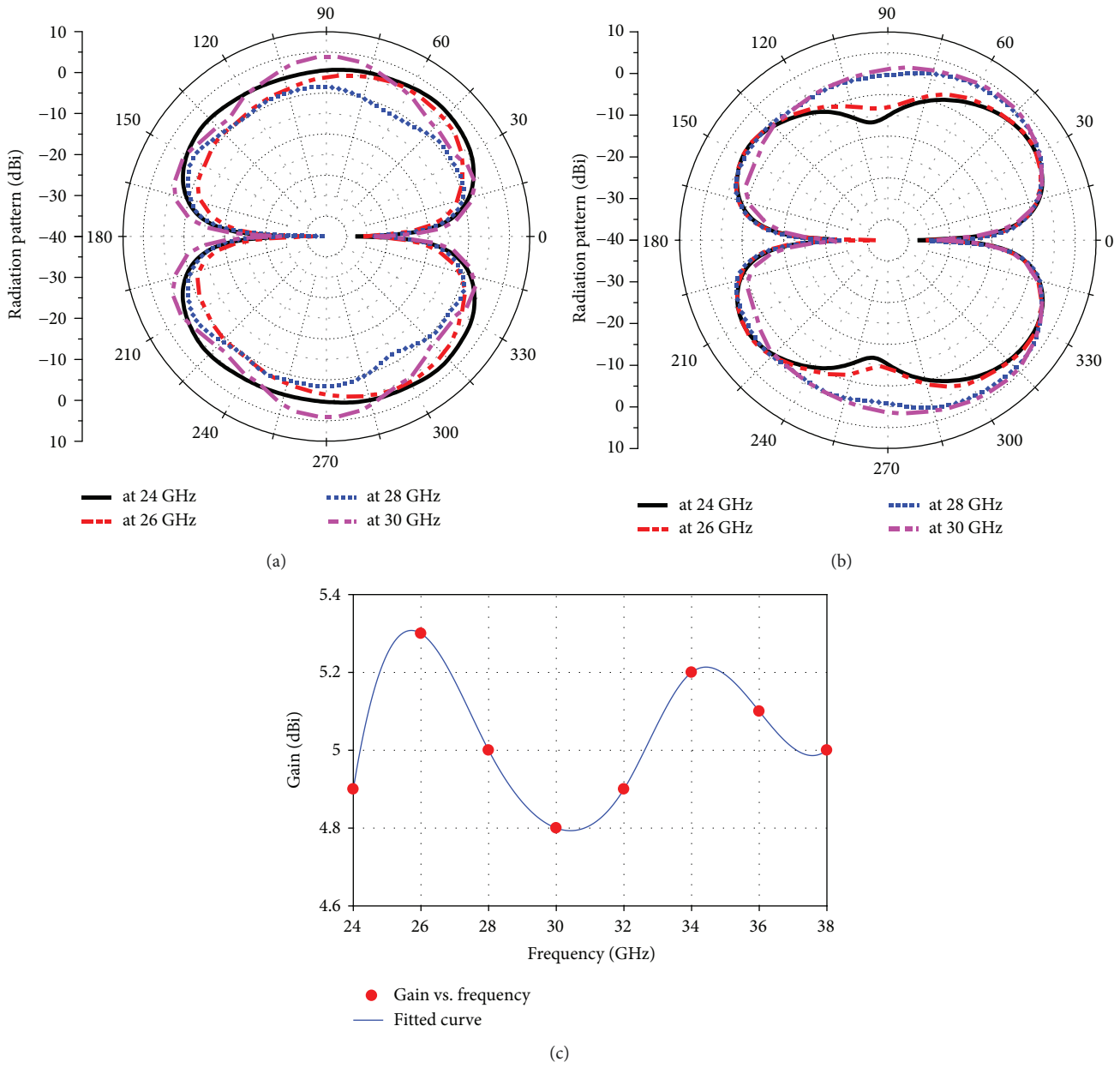

Figure 3: Simulated radiation patterns of the proposed antenna on the xoz-plane (a) and yoz-plane (b), simulated gain of the proposed antenna (c).

radiation energy is first coupled to the parasitic branches and then to the long branches which leads to a weak mutual coupling. For antenna elements 1 and 9, due to the much longer distance and the limitation of the radiation pattern, the energy coupled to them is much lower. Similarly, as shown in Figure 5(b), the radiation is mainly provided by the parasitic branches at 34 GHz. The energy coupled to the antenna elements 4 and 6 is very low, and the energy coupled to the antenna elements 2 and 8 is absorbed by the long branches.

Based on the above antenna, a 9×9 MIMO antenna is developed and depicted in Figure 6(a). The geometry of the single antenna element is as same as shown in Figure 1. The distance between antenna elements is only 0.4 mm which is 0.03 λ_0 (λ_0 refers to the wavelength in free space at 24 GHz). Hence, the S-parameters of the 9×9 MIMO antenna are presented in Figure 6(b). It can be found that the MIMO antenna still resonates from 24 GHz to 37 GHz and the isolation between antenna elements maintains on a high level (the transmission coefficient is under −20 dB) in the operation band.

The simulated three-dimension (3-D) radiation patterns are illustrated in Figure 7. From Figure 7, it can be seen that the radiation of the proposed antenna is much stronger at the z-direction due to its unique structure. This characteristic insures the high isolation within such an extremely close space without introducing external decoupling structure. Besides, the simulated gain of a single antenna element of the MIMO antenna is presented in Figure 7(c). Compared

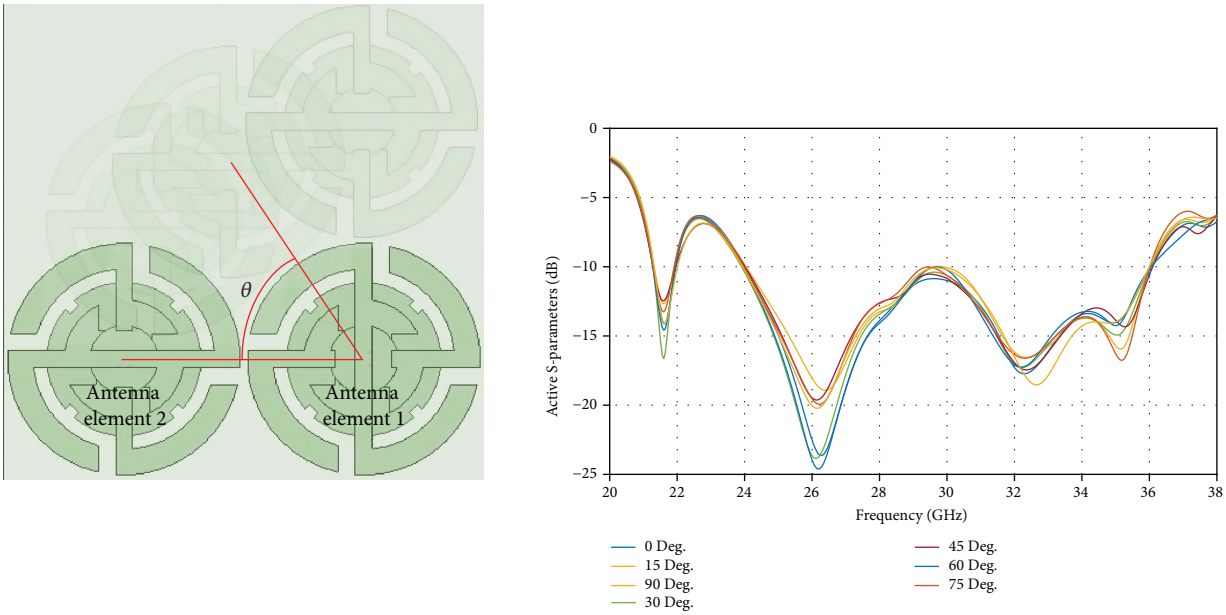

(a) (b)

Figure 4: (a) Geometry and (b) simulated active S-parameters of the MIMO antenna with different angel between two elements.

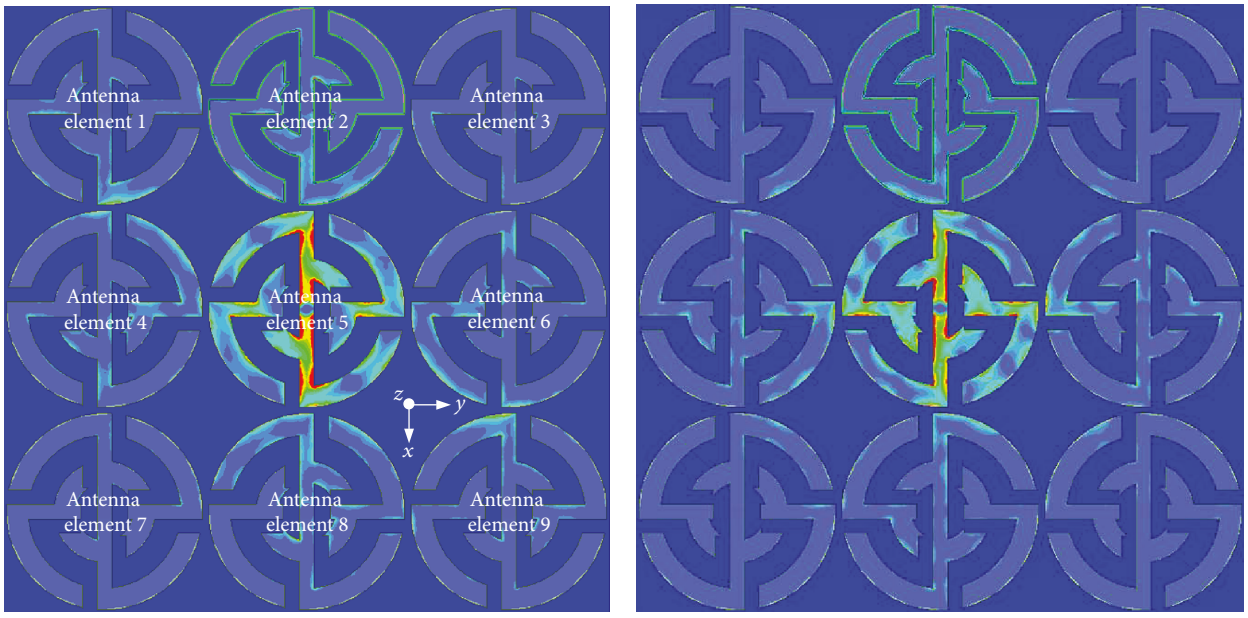

(a) (b)

Figure 5: Surface current distribution on the MIMO antenna at (a) 26 GHz and (b) 34 GHz.

with Figure 3(c), it can be found that due to the benefits from other elements, the maximum gain of a single element reaches 7.5 dBi at 24 GHz.

3. Results and Discussion

In order to verify the designed approaches, a 9×9 MIMO antenna is fabricated. The top and back view of the fabricated sample are presented in Figures 8(a) and 8(b). The zoom-in picture of a single antenna element is included in Figure 8(a). Note that we add an annulus with a width of 0.1 mm around the via on the top side which can help fabrication.

The measured S-parameters are presented in Figure 9. It can be found that the experimental results are in good agreement with the simulated ones. In the experiment, considering the cost and the symmetry of the entire structure, we used 9 K

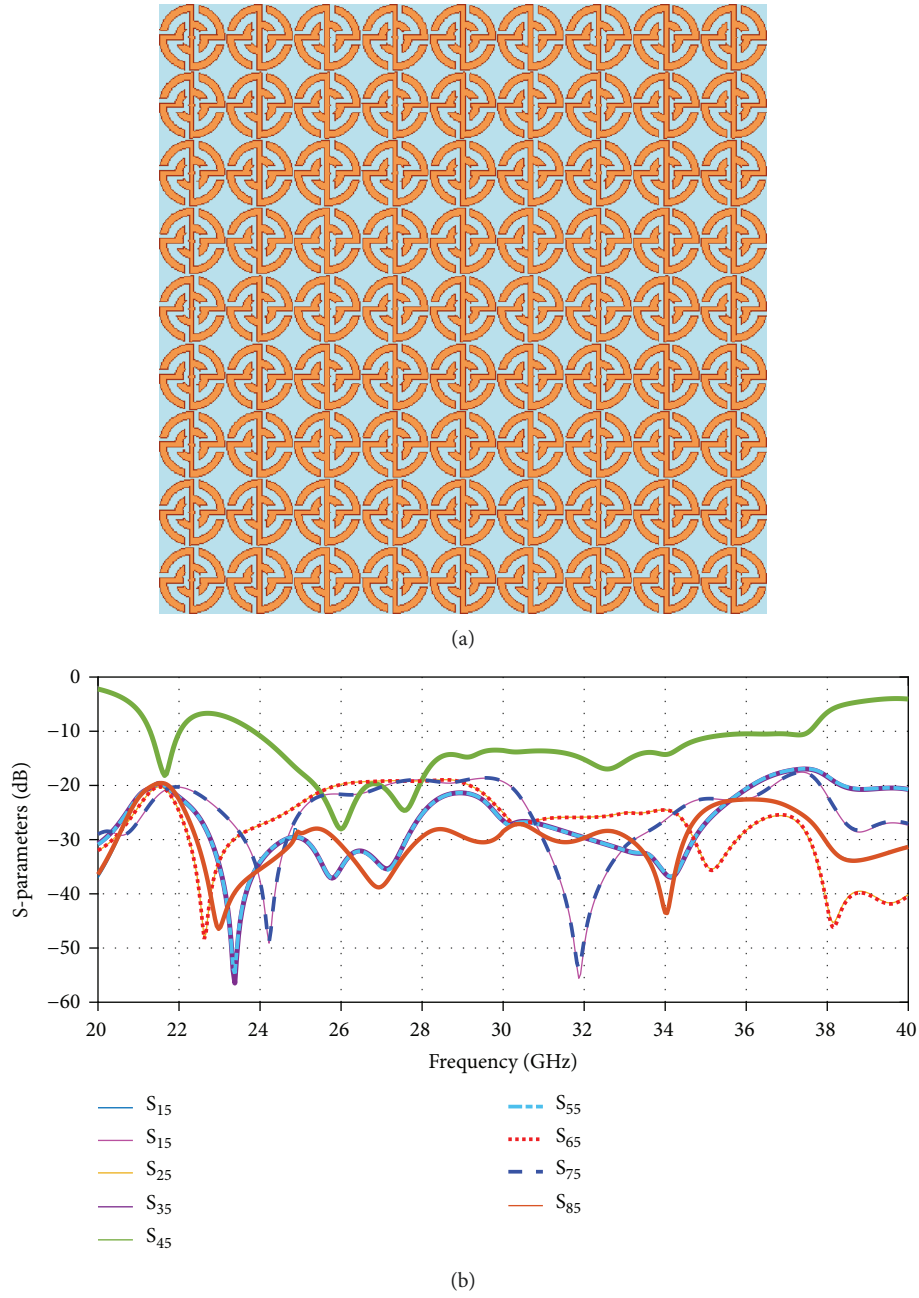

Figure 6: (a) Geometry and (b) S-parameters of the 9 × 9 MIMO antenna.

connectors and connect them to the central ones. Then, we removed them and connected the terminations to the ports on the edge. Compared S_{13} with S_{12}, we can find that the mutual coupling significantly decreases when the distance between the antenna elements increases.

During the radiation pattern measurement, one antenna is excited while the other ones are attached to a 50 Ω load. Note that here, the terminations are only connected to the nearest neighbors since the influence from the distant ones is low enough to be ignored. The measured radiation patterns are presented in Figure 10 which show that the proposed 9 × 9 MIMO antenna has an approximate omnidirectional radiation and the radiation pattern changes slightly in such a wide operation band. Besides, we measured the radiation efficiency of the antenna as shown in Figure 10(c). It can be seen that the radiation efficiency is higher than 65% within the operation band. Therefore, the proposed 9 × 9 MIMO antenna is suitable for cell phones, laptops, and other mobile devices.

To highlight the merits of the proposed MIMO antenna, the comparison between our design and other typical compact MIMO antenna counterparts is given in Table 2. Due to its unique structure, the proposed antenna can realize a high isolation within a much smaller space. Therefore, the size of a

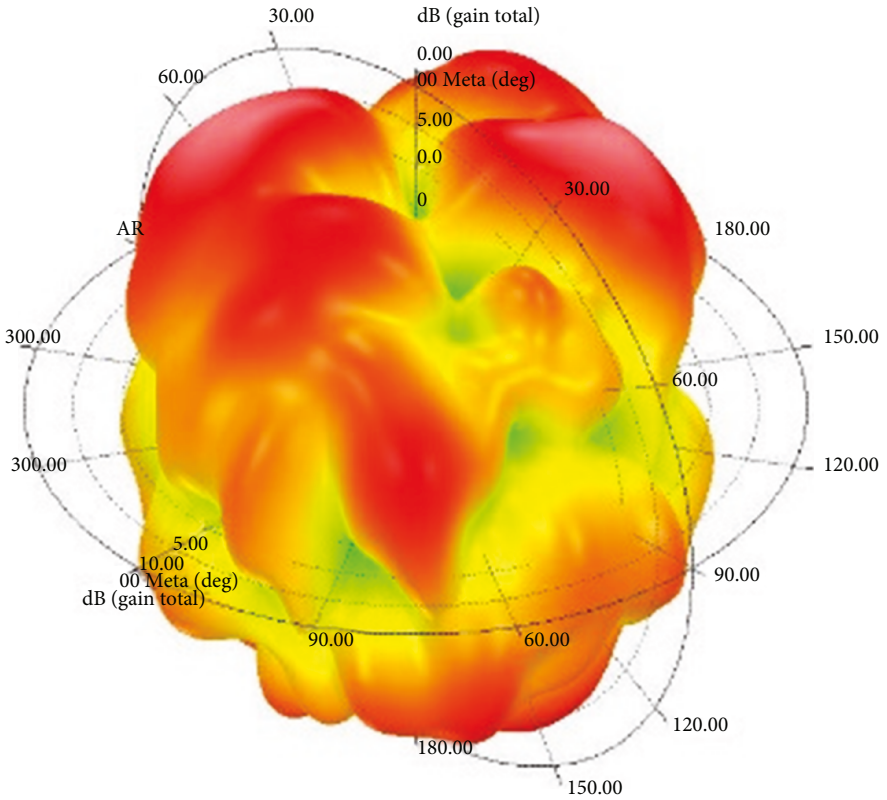

(a)

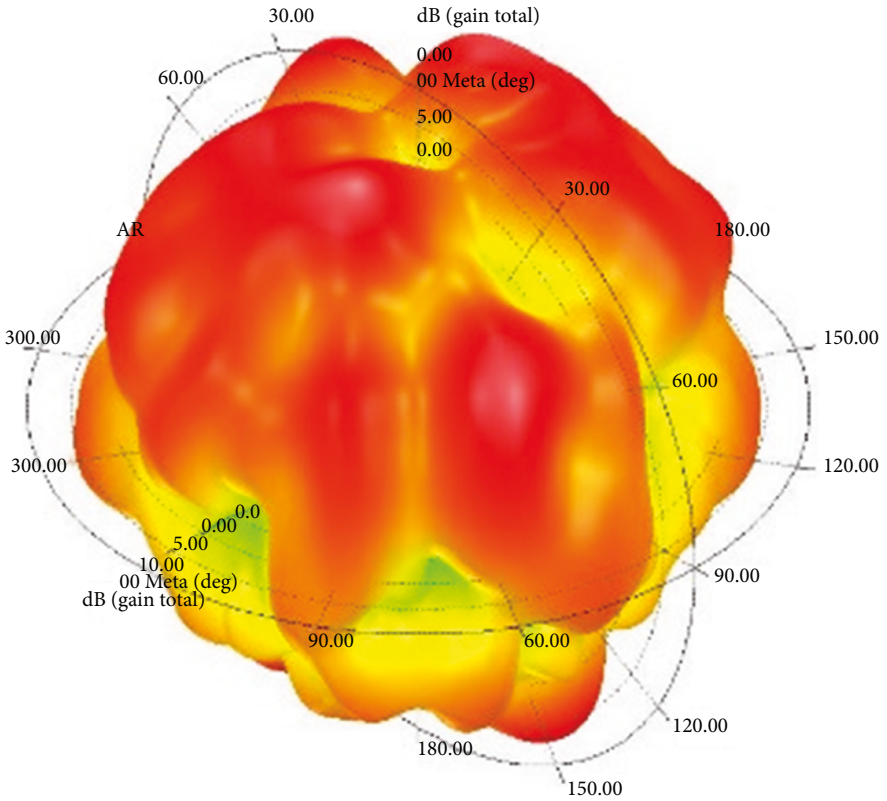

(b)

Figure 7: Continued.

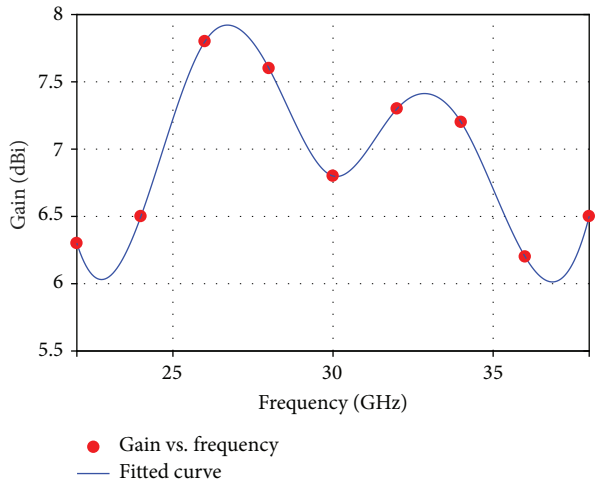

(c)

Figure 7: Simulated 3-D radiation patterns of the 3 × 3 MIMO antenna at (a) 28 GHz and (b) 32 GHz, simulated gain of single element of the proposed MIMO antenna.

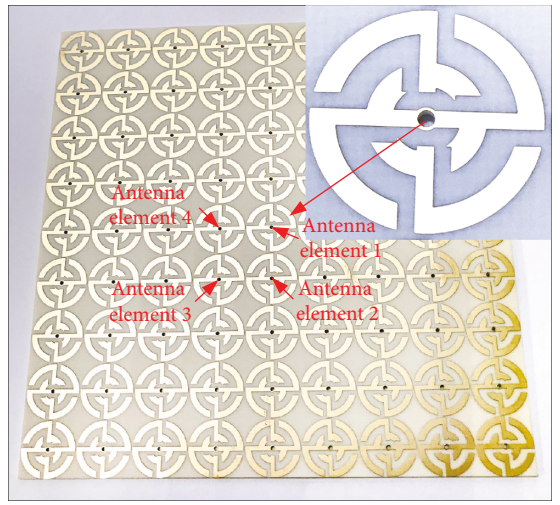

(a)

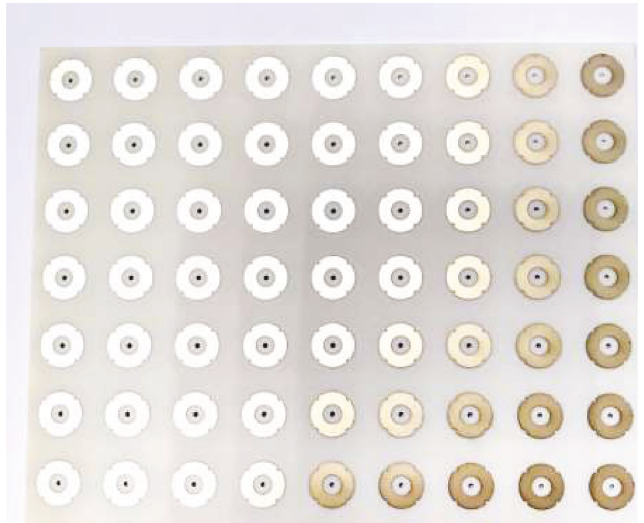

(b)

Figure 8: Top (a) and bottom (b) view of the fabricated 9 × 9 MIMO antenna sample.

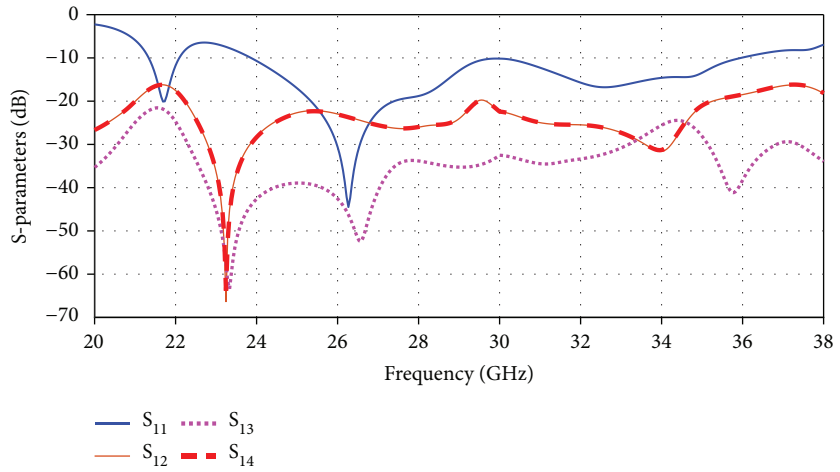

Figure 9: Measured S-parameters of the fabricated MIMO antenna.

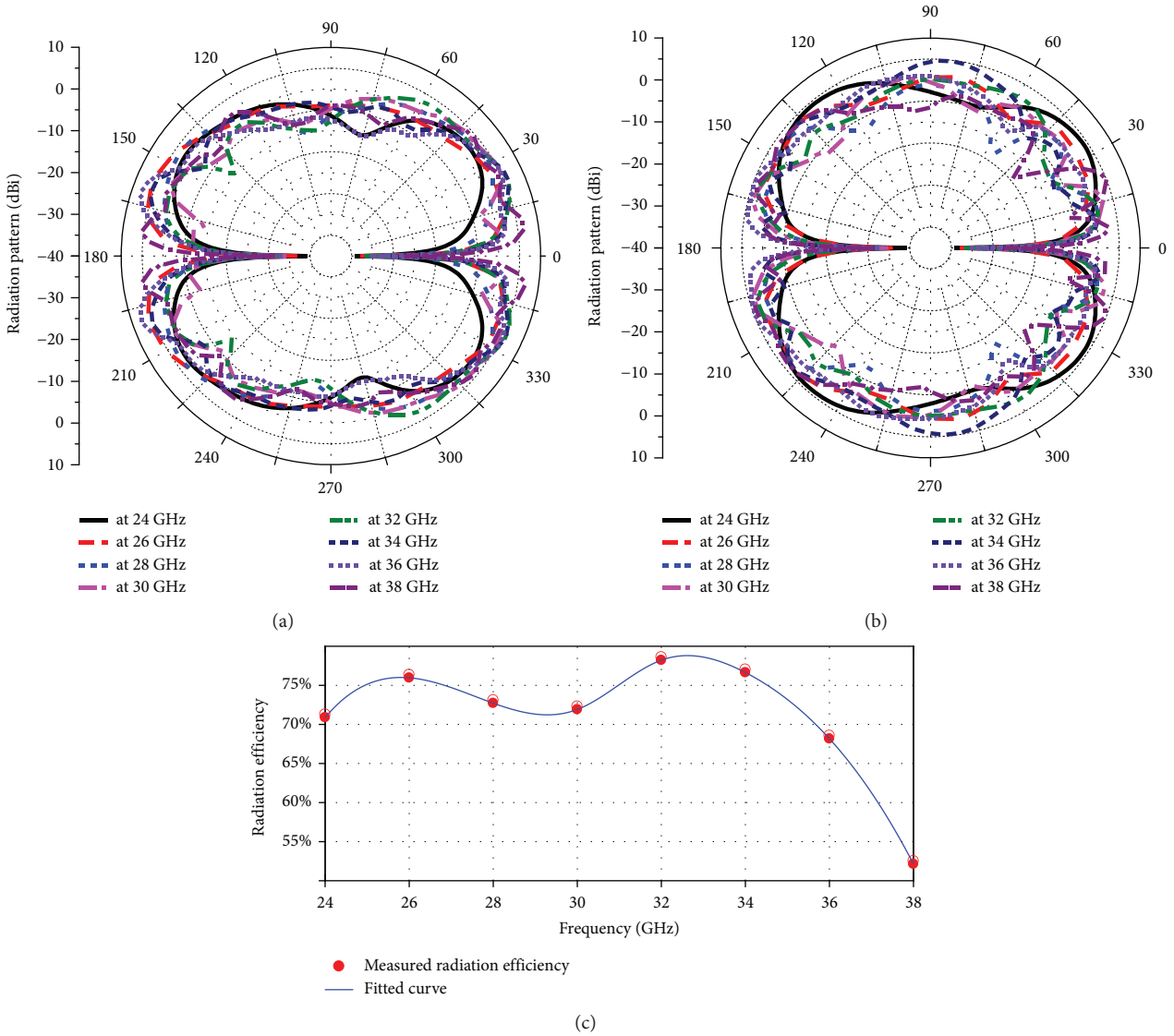

Figure 10: Measured radiation patterns of the proposed antenna on the (a) xoz-plane and (b) yoz-plane; (c) measured radiation efficiency and fitted curve of the antenna.

Table 2: Characteristic parameters of the typical antenna counterparts.

Source	[12]	[13]	[14]	[15]	This paper
Total size (mm)	48×21	12.8×31	42×85	48×31	126×126
Number of ports	2	4	2	4	81
Operating band (GHz)	29.7-31.5	31-40.3	27-32	26-31	24-36
Min isolation (dB)	25	21	37.1	21	20
Peak gain (dBi)	8.6	11	17.9	10	7.8
Edge to edge spacing (λ_0)	$\lambda_0/3.6$	$\lambda_0/1.27$	λ_0	$\lambda_0/6$	$\lambda_0/33$

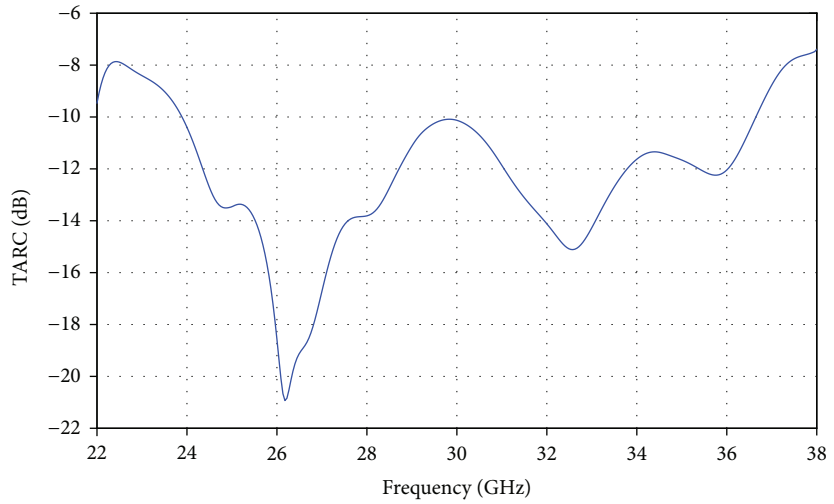

Figure 11: TARC of the proposed MIMO antenna.

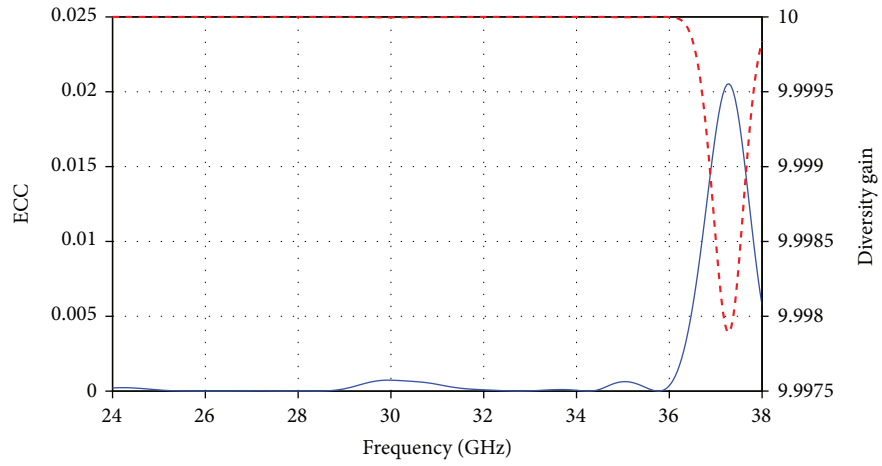

Figure 12: Correlation coefficient and diversity gain of the proposed UWB MIMO antenna.

single antenna element is much smaller than others. Besides, the proposed antenna also shows advantage in wide operation bandwidth and large-scale arrays. However, due to the limitation of the overall size, the peak gain is lower than other works.

The total active reflection coefficient (TARC) is calculated to predict the radiation performance of the MIMO antenna. The TARC can be obtained from the scattering matrix by using the following formula:

$$\Gamma = \frac{\sqrt{\sum_{i=1}^{N} |b_i|^2}}{\sqrt{\sum_{i=1}^{N} |a_i|^2}}, \quad (1)$$

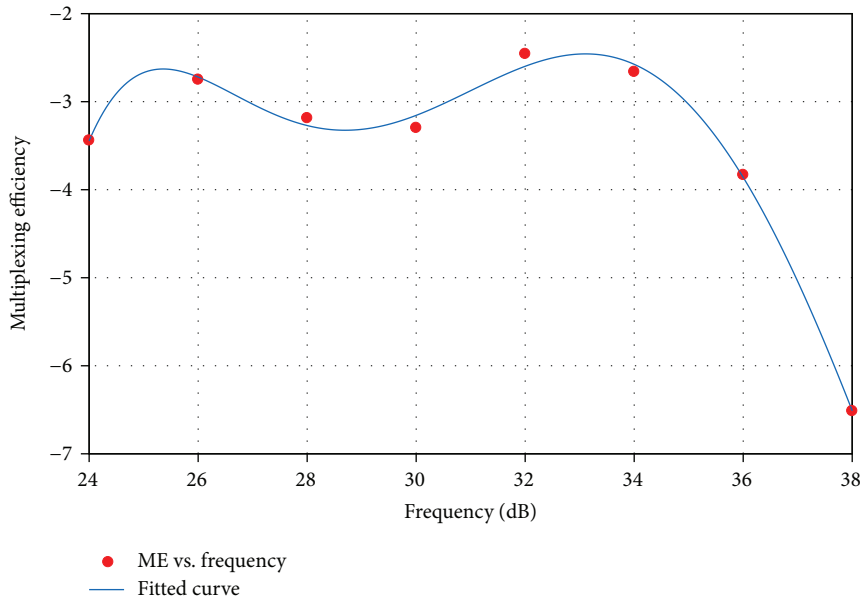

Figure 13: Multiplexing efficiency of the proposed UWB MIMO antenna.

where $b_i = [S] \cdot a_i$. $[S]$ is the scattering matrix of the MIMO antenna, $[a]$ is the excitation vector, and $[b]$ is the scattered vector. The calculated results are illustrated in Figure 11. It is shown that the TARC keeps under -10 dB in the entire operation band.

Moreover, as an important parameter of the MIMO antenna, the enveloped correlation coefficient (ECC) is computed to quantify the isolation among the MIMO antenna elements:

$$\rho_e = \frac{\left| \iint_{4\pi} \left[\overrightarrow{E_1}(\theta,\phi) \cdot \overrightarrow{E_2}(\theta,\phi) \right] d\Omega \right|^2}{\iint_{4\pi} \left| \overrightarrow{E_1}(\theta,\phi) \right|^2 d\Omega \iint_{4\pi} \left| \overrightarrow{E_2}(\theta,\phi) \right|^2 d\Omega}, \quad (2)$$

where $Ei(\theta,\phi)$ refers to the electric field radiated by the antenna element i with the other antenna element terminated by a 50 Ω load. The calculated results are shown in Figure 12. It can be seen that ρ_e is less than 0.005 in the operation band, which indicates the high isolation between antenna elements.

Furthermore, the diversity gain of the proposed MIMO antenna is calculated and presented in Figure 12. The diversity gain can be computed using the following relation:

$$DG = 10\sqrt{1 - |\rho_e|^2}. \quad (3)$$

In Figure 12, it can be found that the diversity gain is close to the ideal value (10) in the entire operation band which also proves the success of our design.

Finally, as another important parameter to evaluate the MIMO antenna performance, the multiplexing efficiency is calculated by using the formula as follows:

$$\eta = \sqrt{\left(1 - |\gamma|^2\right)\eta_1\eta_2}, \quad (4)$$

where η_1 and η_2 refer to the measured radiation efficiencies of the two antenna elements, respectively. γ refers to the correlation between antenna elements. The calculated multiplexing efficiency is illustrated in Figure 13. From Figure 13, it can be seen that the multiplexing efficiency is above −4 dB in the operation band.

4. Conclusions

In this letter, a wideband MIMO antenna with high isolation is proposed and studied. Due to its unique structure, the proposed antenna can achieve high isolation (under −20 dB) within an extreme closed space (0.4 mm) without any extra decoupling structure. Also, the simulated results show that the proposed antenna structure can be composed into different MIMO antenna structure as needed. The experimental results show that the proposed antenna has obvious advantages such as stable radiation pattern, wide operation bandwidth, and high isolation. The proposed antenna has potential applications in the next generation communication.

Data Availability

No data were used to support this study.

Conflicts of Interest

The authors declare that there is no conflict of interest regarding the publication of this paper.

Acknowledgments

This work was supported in part by the National Natural Science Foundation of China (Grant Nos. 6147109, 61611130067, and 61531010).

References

[1] W. Roh, J. Y. Seol, J. Park et al., "Millimeter-wave beamforming as an enabling technology for 5G cellular communications: theoretical feasibility and prototype results," *IEEE Communications Magazine*, vol. 52, no. 2, pp. 106–113, 2014.

[2] J. G. Andrews, S. Buzzi, W. Choi et al., "What will 5G be?," *IEEE Journal on Selected Areas in Communications*, vol. 32, no. 6, pp. 1065–1082, 2014.

[3] P. Wang, Y. Li, L. Song, and B. Vucetic, "Multi-gigabit millimeter wave wireless communications for 5G: from fixed access to cellular networks," *IEEE Communications Magazine*, vol. 53, no. 1, pp. 168–178, 2015.

[4] T. S. Rappaport, Y. Xing, G. R. MacCartney, A. F. Molisch, E. Mellios, and J. Zhang, "Overview of Millimeter Wave Communications for Fifth-Generation (5G) Wireless Networks-with a focus on Propagation Models," *IEEE Transactions on Antennas and Propagation*, vol. 65, no. No. 12, pp. 6213–6230, 2017.

[5] J. R. Costa, E. B. Lima, C. R. Medeiros, and C. A. Fernandes, "Evaluation of a new wideband slot array for MIMO performance enhancement in indoor WLANs," *IEEE Transactions on Antennas and Propagation*, vol. 59, no. 4, pp. 1200–1206, 2011.

[6] A. Mchbal, N. Amar Touhami, H. Elftouh, and A. Dkiouak, "Mutual coupling reduction using a protruded ground branch structure in a compact UWB owl-shaped MIMO antenna," *International Journal of Antennas and Propagation*, vol. 2018, Article ID 4598527, 10 pages, 2018.

[7] Z. Y. Li, Z. W. Du, M. Takahashi, K. Saito, and K. Ito, "Reducing mutual coupling of MIMO antennas with parasitic elements for mobile terminals," *IEEE Transactions on Antennas and Propagation*, vol. 60, no. 2, pp. 473–481, 2012.

[8] S. Assimonis, T. Yioultsis, and C. Antonopoulus, "Design and optimization of uniplanar EBG structures for low profile antenna applications and mutual coupling reduction," *IEEE Transactions on Antennas and Propagation*, vol. 60, no. 10, pp. 4944–4949, 2012.

[9] Y. Lee, D. Ga, and J. Choi, "Design of a MIMO antenna with improved isolation using MNG metamaterial," *International Journal of Antennas and Propagation*, vol. 2012, Article ID 864306, 7 pages, 2012.

[10] N. K. Kiem, H. N. B. Phuong, Q. N. Hieu, and D. N. Chien, "A novel metamaterial MIMO antenna with high isolation for WLAN applications," *International Journal of Antennas and Propagation*, vol. 2015, Article ID 851904, 9 pages, 2015.

[11] J. Liu, K. P. Esselle, S. G. Hay, Z. Sun, and S. Zhong, "A compact super-wideband antenna pair with polarization diversity," *IEEE Antennas and Wireless Propagation Letters*, vol. 12, pp. 1472–1475, 2013.

[12] M. S. Sharawi, S. K. Podilchak, M. T. Hussain, and Y. M. M. Antar, "Dielectric resonator based MIMO antenna system enabling millimetre-wave mobile devices," *IET Microwaves, Antennas & Propagation*, vol. 11, no. 2, pp. 287–293, 2017.

[13] Y. W. Hsu, T. C. Huang, H. S. Lin, and Y. C. Lin, "Dual-polarized quasi Yagi-Uda antennas with endfire radiation for millimeter-wave MIMO terminals," *IEEE Transactions on Antennas and Propagation*, vol. 65, no. 12, pp. 6282–6289, 2017.

[14] S. Gupta, Z. Briqech, A. R. Sebak, and T. A. Denidni, "Mutual-coupling reduction using metasurface corrugations for 28 GHz MIMO applications," *IEEE Antennas and Wireless Propagation Letters*, vol. 16, pp. 2763–2766, 2017.

[15] Z. Wani, M. P. Abegaonkar, and S. K. Koul, "A 28-GHz antenna for 5G MIMO applications," *Progress In Electromagnetics Research Letters*, vol. 78, pp. 73–79, 2018.